# High Spatial Resolution Satellite Imagery, DEM Derivatives, and Image Segmentation for the Detection of Mass Wasting Processes

**John Barlow, Steven Franklin, and Yvonne Martin**

## Abstract

*An automated approach to identifying landslides using a combination of high-resolution satellite imagery and digital elevation derivatives is offered as an alternative to aerial photographic interpretation. Previous research has demonstrated that per pixel spectral response patterns are ineffective in discriminating mass movements. This technique utilizes image segmentation and digital elevation data in order to identify mass movements based not only on their reflectance but also on their shape properties and their geomorphic context. Dividing the classification by process into debris slides, debris flows, and rock slides makes the method far more useful than methods that group all mass movements together. A hierarchical classification scheme is utilized to eliminate areas that are not of interest and to identify areas where mass movements are probable. A supervised classification is then conducted using spectral, shape, and textural properties to identify failures that were greater than 1 ha in area. The resulting accuracy was 90 percent for debris slides, 60 percent for debris flows, and 80 percent for rock slides.*

## Introduction

Landslide inventories are increasingly recognized as a useful geomorphic research tool for landslide hazard assessments (e.g., Baeza and Corominas, 2001), for the determination of process rates in sediment budget studies (e.g., Campbell and Church, 2004; Martin *et al.*, 2002), and for calibrating long-term landscape evolution models (e.g., Martin, 2000). Mass wasting is widely recognized as the key process by which sediment is delivered to the fluvial subsystem within alpine areas (Hovius *et al.*, 1997; Jacob, 2000). The determination of process rates has therefore been a central theme within the research literature (e.g., Brardinoni and Church, 2004; Guthrie and Evans, 2004; Guzzetti *et al.*, 2002). Process rate assessment requires an inventory of mass wasting events over large spatial scales, typically using aerial photographs to identify failures. However, aerial photographic interpretation efforts are often time consuming and are subject to highly variable degrees of accuracy depending both on the experience of the analyst and the scale and quality of the photographs (Brardinoni *et al.*, 2002). It is therefore critical to establish a technique that is able to rapidly establish the rates of mass movements over large areas with known levels of accuracy in order to facilitate meaningful comparisons between regions of differing geological and climactic boundary conditions.

The identification of mass movements using satellite remote sensing and digital elevation data has been addressed numerous times within the research literature. Early work suggested that relatively coarse spatial resolution per pixel spectral response patterns, when used alone, are unreliable in discriminating landslide scars from other barren areas on the landscape (e.g., Sauchyn and Trench, 1978; Epp and Beaven, 1988). For this reason, other researchers have attempted to use a combination of both satellite imagery and digital elevation models (DEMs) (e.g., Giles *et al.*, 1994; McDermid and Franklin, 1995; Giles and Franklin, 1998). McDermid and Franklin (1995) noted that, in many cases, per pixel reflectance patterns are unrelated to geomorphic process and classification schemes based on this data would fail. They suggested that a combination of geomorphometric criteria as well as spectral data would yield better results in identifying mass movement features. More recently, Barlow *et al.* (2003) used a combination of image segmentation with Landsat ETM+ and DEM data to identify translational landslide scars; the overall accuracy was 75 percent. However, the detection and classification of individual process types (Cruden and Varnes, 1996) using an automated approach has been less successful. Martin and Franklin (2005) demonstrated that textural analysis of landslide scars may be capable of discriminating between rock slides and debris slides although the spatial resolution of image data was a limiting factor.

The objective of this research is to develop an automated classification scheme capable of identifying different classes of rapid mass movements from a digital database composed of high spatial resolution SPOT 5 imagery and a digital elevation model. Fresh mass wasting events over 1 ha in size are considered in the accuracy assessment. The size criterion was deemed necessary as smaller failures become increasingly difficult to identify on aerial photographs (Brardinoni and Church, 2004). Accuracy assessment for smaller failures based on aerial photographs would therefore be problematic (Congalton, 1991). The landslide classification system given by Cruden and Varnes (1996)

John Barlow and Yvonne Martin are with the Department of Geography, University of Calgary, 2500 University Drive, NW, Calgary, Alberta Canada, 2TN 1N4 (jbarlow@ucalgary.ca; ymartin@ucalgary.ca).

Steven Franklin is the Vice-President of Research, University of Saskatchewan (Steven.Franklin@usask.ca).

Photogrammetric Engineering & Remote Sensing
Vol. 72, No. 6, June 2006, pp. 687–692.

0099-1112/06/7206–0687/$3.00/0

was utilized. This system emphasizes the type of movement and the type of material involved such that:

- Debris slides are defined as failures in coarse-grained surface material occurring predominantly across a rupture surface.
- Rock slides involve predominantly hard, intact, bedrock masses failing along a plane of intense shear strain.
- Debris flows occur when coarse-grained surface material is saturated to such a degree that movement is initiated down slope due to gravity.

These classes are not mutually exclusive nor are they exhaustive. Debris flows can initially start out as debris slides or vise versa, depending on the level of saturation and the slope gradient (Cruden and Varnes, 1996; Iverson, 1997). Furthermore, rock slides will undoubtedly entrain unconsolidated surface material while debris slides often show some inclusion of bedrock in their deposits. Classification using the traditional methods involving aerial photography is understandably subjective to some extent and will produce variable results between individuals. One of the potential advantages of an automated approach lies in objective use of quantitative data in the classification process making comparisons between areas more viable.

## Study Area

The classification was applied to a 440 km$^2$ area of the Chilliwack River Basin, (Figure 1). Of this, less that 1 percent is representative of fresh landslides. The basin is located approximately 160 km east of Vancouver on the border between Canada and the United States. The Chilliwack River flows west from Lake Chilliwack with smaller tributary valleys feeding in from the north and south. The elevation ranges from 13 m above sea level where the valley opens out onto the Fraser River floodplain to a maximum of 2,283 m with many peaks exceeding 2,000 m. The climate offers warm, dry summers and cool, wet winters. Mean annual precipitation is 1,500 mm although this is doubtless higher on peaks and high passes. A maximum daily rainfall of 99.6 mm was reported for the 40-year period of record between 1962 and 2002 (Environment Canada, 2005). The geology of the area is complex with the western portion being primarily mudstone and sandstone of the Cultis Formation, the central portion of the basin is underlain by a series of volcanic rocks, mudstone, sandstone, and limestones of the Chilliwack Group, while the granodiorite and quartz diorite are common in the eastern part of the basin (Massey *et al.*, 2004). The pattern of deglaciation at the end of the Pleistocene was complex and has been described in detail by Saunders *et al.* (1987). Radiocarbon dating of woody deposits indicates that the area was ice-free by about 11,100 years BP (Saunders *et al.*, 1987). The basin strongly reflects the glacial processes of the Pleistocene with many drift mantled and oversteepened slopes. This combination of steep, drift mantled slopes and high precipitation makes mass wasting a common occurrence. The area is also subject to extensive logging operations with clear cuts evident on all but the steepest of valley slopes and a network of logging roads running though all the tributary valleys.

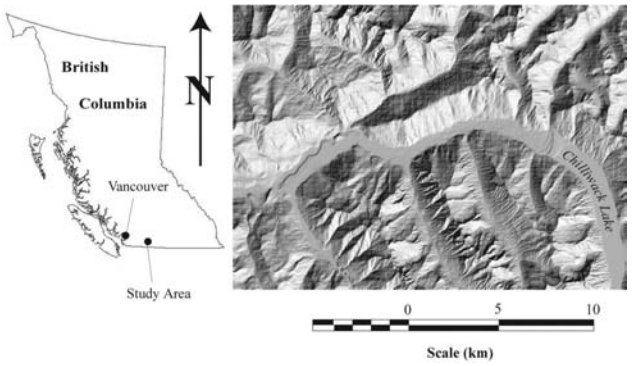


Figure 1. Chilliwack Study Area.

## Data Input

Panchromatic and multispectral SPOT 5 data acquired on 27 September 2004 and digital elevation data were used as the input for the automated classification. The satellite data consisted of a 2.5 m resolution panchromatic band (0.49 to 0.69 $\mu$m) and four 10 m resolution spectral bands including green (0.49 to 0.61 $\mu$m), red (0.61 to 0.68 $\mu$m), near infrared (0.78 to 0.89 $\mu$m), and short wave infrared (1.58 to 1.75 $\mu$m). The red and near infrared spectral bands were used to create a normalized difference vegetation index (NDVI) layer. NDVI values have shown a correlation with green leaf biomass and green leaf area (Kidwell, 1990) and are useful in assessing the presence of vegetation in a given area. A DEM derived from 1:50 000 scale topographic maps of the Chilliwack Basin was acquired from the Canadian Centre for Topographic Information (Geobase, 2005) and rescaled to a 25 m pixel size. Jones (1998) demonstrated that the method described by Horn (1981) provides reliable approximations of the surface derivatives. Image layers of slope tangent and plan convexity, both known to be of importance in the initiation of landslides (Gao, 1993), were calculated and added to the database. The final data layer used was relief. This layer was created following image segmentation and gives values representing the maximum change in elevation for the spatial extent of each polygon.

A manual inventory of rapid mass movements was undertaken using color 1:15 000 scale aerial photographs acquired in July 1996. Failures were identified under a 10× power stereoscope. Failures were classified as debris slides, debris flows, or rock slides. Due to the time difference between the acquisition of the photographs and the satellite imagery, the panchromatic band was inspected manually, and fresh failures were identified and added to the inventory. Within the classification, fresh failures are defined as having an NDVI value of less than 0.15, in reality, this roughly equates to those failures that have occurred within the past 10 years. Surface observations to support the inventory obtained via aerial photographic interpretation were collected during the summer of 2002.

## Methods

### Segmentation

Image segmentation was accomplished using the eCognition software environment (Definiens, 2005). The segmentation algorithm is calibrated using user-defined threshold of scale and heterogeneity and user-defined weightings on the various data layers (Chubey *et al.*, 2005). This is generally an iterative process whereby the user can attempt a series of scaling combinations such that the created polygons are large enough to capture features of interest. However, the creation of polygons that accurately represent landslide features is problematic as the area of the failures varies across several orders of magnitude. Therefore, no one scaling parameter will be able to accurately represent the entire population. This problem can be largely solved through

multiresolution segmentation (Definiens, 2005). This allows the merging of adjacent polygons based on a spectral heterogeneity criterion. An initial segmentation set at a small scale in order to capture the smaller failures (1 ha) can be used as a basis for further segmentation layers. Objects are merged if they do not exceed a heterogeneity threshold such that larger slides come to be represented by one large polygon whereas the smaller ones do not merge with their neighboring polygons as the heterogeneity criterion is exceeded. The segmentation that proved the most effective at capturing mass wasting events within the study area relied on an equal weighting of the spectral bands as well as the plan curvature layer. The value of image segmentation lies in the subsequent ability to look at the objects both in their context within the landscape as well as their innate shape properties. This offers great advantages over classification using per pixel spectral response patterns alone.

#### Classification Hierarchy

The data layers used and the classification hierarchy are illustrated in Figure 2. The image classification scheme is similar to that employed by Barlow *et al.* (2003). Image objects that are not of interest are progressively eliminated by four boolean decision criteria. In essence, this mimics the procedure used during photographic interpretation and focuses attention on unvegetated portions of steep slopes that display the appropriate shape characteristics and orientation.

The first step in the classification is the separation of objects into vegetated/unvegetated classes based on an NDVI threshold of 0.15. Those objects that have an NDVI value greater than this are classified as vegetated, and therefore eliminated from consideration. This accounts for over half of the image objects in the study area. The next level assigns each of the unvegetated image objects to either flatland or steepland based on the slope layer. Here, the threshold between the two was set at 0.27 (15 degrees), as no rapid mass movements were observed in the field below this gradient. All of the objects that were classified as steepland were then evaluated based on a length to width shape criterion. Mass movements are generally identified as long thin features. Empirical inspection of the aerial photographic inventory demonstrated that mass movements had a length to width ratio of 2.5 or higher. Therefore, this threshold was required to be classified as a thin feature, while the remaining objects were classified and labeled as *square features*.

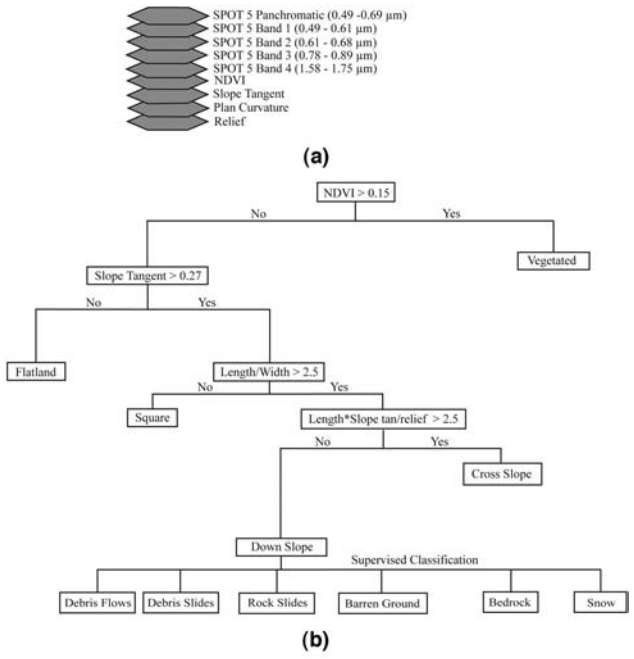


Figure 2. Classification schematic showing data layers (a) and the classification hierarchy (b). Note: not all image layers are used in the supervised classification, see text for details.

The resulting polygons were a group of unvegetated areas located on steeper slopes with long, thin shape properties. Barlow *et al.* (2003) found that by using the spectral properties of such polygons, a fairly accurate classification of landslides was possible. However, errors of commission were high with objects such as roads and talus slopes. One of the most obvious characteristics of rapid mass movements is their dependence on gravity. Failure tracks tend to follow the path of steepest descent (fall line) down a given slope. The geomorphic context of an image object is therefore a useful tool in the classification. The orientation of the long axis of an object on the slope was used to separate those that ran roughly parallel to the fall line to those that extend across the slope. Theoretically, for a landslide on an infinite slope:

$$\frac{L \tan \beta}{\Delta z} = 1 \qquad (1)$$

where $L$ is the horizontal or projected length of the landslide, $\beta$ is slope, and $\Delta z$ is the change in elevation from the top of the initiation zone to the toe of the landslide. Applying this formula to objects in the study area was problematic, as eCognition does not have the functionality to determine $\Delta z$. Therefore, the "thin" polygons were first exported into ArcView® and assigned a relief based on the DEM. This was then rasterized and input into eCognition as the "relief" data layer. The mean value assigned by eCognition to each of the image objects was therefore equivalent to the maximum change in elevation ($\Delta z$) from Equation 1. Of course, in the real world, slopes are not infinite and the momentum of a failed mass can cause it to deviate from the fall line. For this reason, a threshold of 2.5 was set in the classification hierarchy.

Applying Equation 1 to the thin image objects within the study area proved to be remarkably effective at removing objects, such as roads, that are very difficult to distinguish from debris slides both in terms of their shape properties and their reflectance (Barlow *et al.*, 2003). Plate 1 shows a portion of the study area with both logging roads and debris slides in close proximity. Due to their orientation on the slope, the logging roads were classified as cross-slope objects, whereas the slides were successfully classified as down-slope objects.

The remaining segments were classified as debris slides, debris flows, rock slides, barren ground, bedrock or snow according to their spectral, shape, and textural characteristics (Figure 2). While the NDVI layer was useful in separating image objects into vegetated and unvegetated classes, its usefulness as a class descriptor for the supervised classification was low. It was therefore omitted from this phase in the classification hierarchy. A supervised classification scheme was adopted whereby a group of sample objects was used to train the classifier. In addition to the mean spectral and geomorphometric values, an asymmetry shape criteria was used that compares the long and short axis of each polygon. The greater the difference, the more asymmetrical an object becomes. This proved useful in discriminating between mass

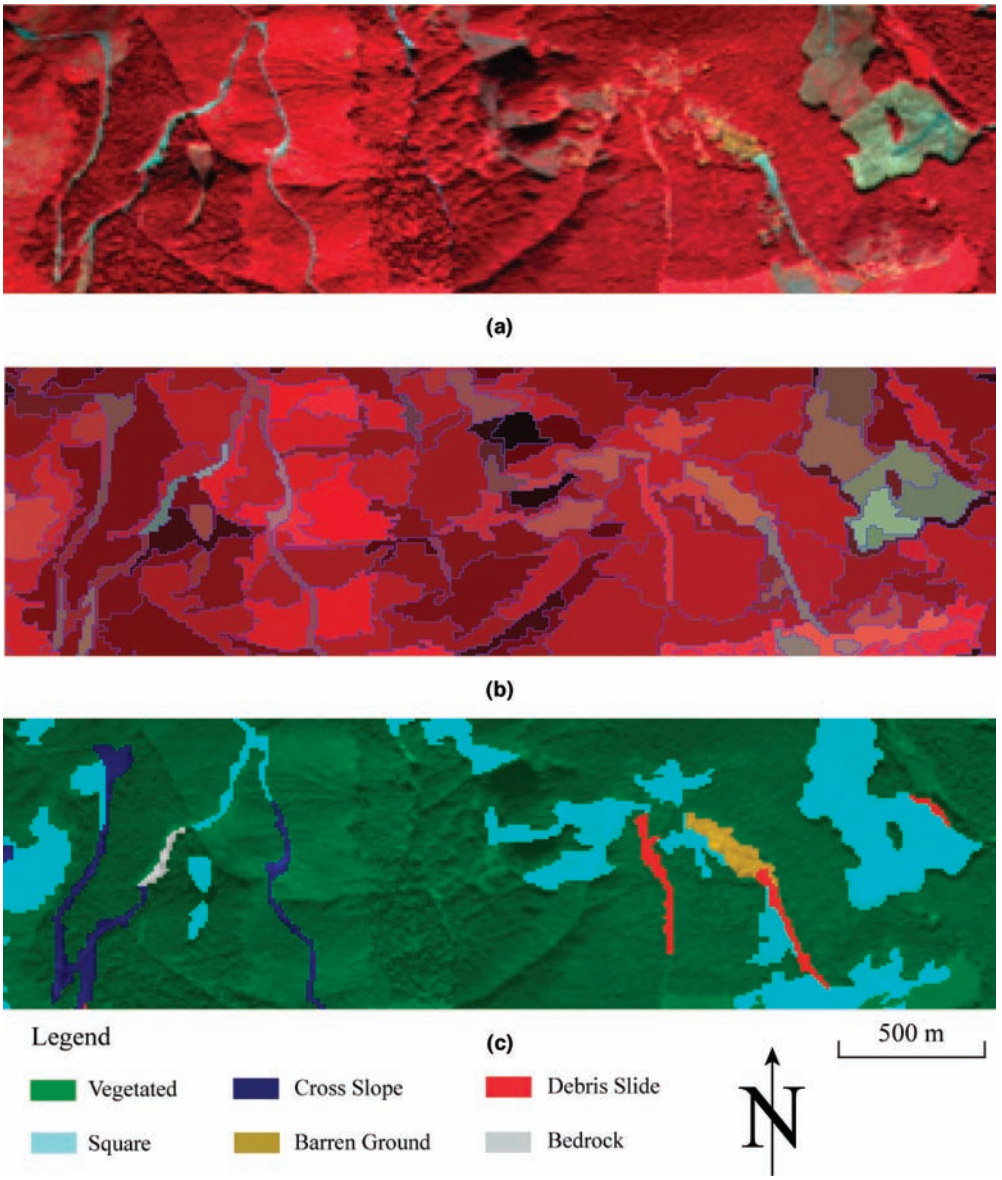


Plate 1. An example of the steps taken in the classification process. (a) denotes the raw imagery, (b) the imagery after segmentation into image objects, and (c) shows a portion of the classified imagery. Note the successful discrimination of the debris slides on the right of the image from the roads on the left. Part of the road system has been misclassified as bedrock.

movements and the barren land class. Finally, the textural properties of homogeneity, dissimilarity, mean, and variance described by Haralick *et al.* (1973) were used to help distinguish between classes. These were applied to the panchromatic band as its 2.5 m resolution captures more spatial detail than that of the 10 m multispectral bands.

## Results and Discussion

The classification system proved to be effective at placing image objects into their geomorphic context with relation to mass wasting. A quantitative accuracy assessment was accomplished by comparing the classified imagery with the landslide inventory compiled from aerial photographs and field observations. Standard confusion matrices (Congalton, 1991) are largely inapplicable to this type of classification scheme as many of the classes are based on shape or morphometric criteria that can be represented by a multitude of differing land-cover types. For this reason, accuracy was only assessed for the mass movement classes. Errors of omission were assessed by taking a random sample of 20 debris slides, 20 debris flows, and 20 rock slides identified from the aerial photographs. These were then compared to the classified imagery. The results of this analysis are shown in Table 1. Fifty percent of the error associated with the classification was interpreted on the resulting image products to originate in a misclassification of process rather than identifying a mass movement feature as some other feature. Similarly, errors of commission were assessed by a random sample of 20 events from each process type on the

TABLE 1. CLASSIFICATION ACCURACY ASSESSMENT FOR ERRORS OF OMISSION. THE ACCURACY WAS DETERMINED BY RANDOMLY SELECTING 20 FAILURES OF EACH TYPE FROM THE AERIAL PHOTOGRAPHS AND COMPARING THEM TO THE CLASSIFIED IMAGE

| | Debris Slide | Rock Slide | Debris Flow |
|---|---|---|---|
| Debris Slide | 18 | 2 | 2 |
| Rock Slide | 0 | 16 | 2 |
| Debris Flow | 1 | 0 | 12 |
| Barren Ground | 1 | 1 | 0 |
| Bedrock | 0 | 1 | 2 |
| Snow | 0 | 0 | — |
| % Accuracy | 90 | 80 | 60 |

TABLE 2. CLASSIFICATION ACCURACY ASSESSMENT FOR ERRORS OF COMMISSION. THE ACCURACY WAS DETERMINED BY TAKING 20 FAILURES OF EACH TYPE FROM THE CLASSIFIED IMAGE AND COMPARING THEM TO THE AERIAL PHOTOGRAPHS

| | Debris Slide | Rock Slide | Debris Flow |
|---|---|---|---|
| Debris Slide | 16 | — | 1 |
| Rock Slide | 1 | 16 | — |
| Debris Flow | 1 | 2 | 16 |
| Barren Ground | 2 | 1 | — |
| Bedrock | — | — | 2 |
| Road | — | — | 1 |
| Vegetated | — | 1 | — |
| % Accuracy | 80 | 80 | 80 |

classified imagery and comparing them to the aerial photographs. There appeared to be few errors of commission between roads and landslide features. This was a significant source of error in the prior research involving image segmentation (Barlow *et al.*, 2003) and therefore represents a great improvement.

#### Debris Slides

At 10 percent omission and 20 percent commission error, debris slides were the class of feature with the highest accuracy achieved in the classification. This could be attributed to the fact that such features are usually situated on open slopes and are characterized by breaks in vegetation. Also, as the debris slide deposit is typically less coarse than those associated with rock slides and debris flows, the textural properties captured in the high spatial resolution imagery appeared to provide a basis for good separation between this class and the others (see Martin and Franklin, 2005). Barren ground proved to be the most problematic source of classification errors, although misclassification as debris flow also resulted in some error.

#### Rock Slides

This type of mass movement also received a high accuracy assessment although there was some misclassification with debris flows, barren ground, and bedrock. Possibly, this is mainly due to the similarities of the spectral and textural characteristics of these features. For example, Martin and Franklin (2005) noted that rockslides are generally larger and wider than debris slides; in the present study, the asymmetry shape criteria appeared to provide some separation between rock slides and debris slides/flows within the class descriptions.

#### Debris Flows

Classification of debris flows proved problematic, likely due to their positioning on the landscape in this study area. They generally occurred in deep mountain gully systems that were often obscured by shadow. This resulted in problems with the image segmentation as the debris flows were often broken up into several shorter segments. While the inclusion of plan curvature in the image segmentation alleviated this to some degree, many were designated as *square features* (as opposed to the long thin features in the classification hierarchy). Additionally, the shadow was often misclassified as vegetated due to a higher NDVI measure compared to observations on exposed bare slopes. However, the classification was capable of achieving an 80 percent accuracy for errors of commission meaning that the criteria set forth in the supervised classification stage were effective in discriminating between the process types. In particular, plan curvature was an excellent class descriptor for debris flows due to their occurrence in areas of high concavity.

## Conclusions

We used image segmentation on a combination of SPOT 5 and DEM data to develop an automated system to detect and classify rapid mass movements that were fresh and over 1 ha in area in a high mountain region in British Columbia. The method improves upon previous attempts (Barlow *et al.*, 2003; Martin and Franklin, 2005) in that the spatial resolution of the spectral data was much greater than that available with Landsat ETM+ imagery and a more robust set of geomorphometric variables were utilized. The method yielded an overall accuracy of 77 percent for all rapid mass movements. These features were further divided according to the classification system of Cruden and Varnes (1996) into debris slides, debris flows, and rockslides; the process specific classification accuracies were 90 percent, 60 percent, and 80 percent respectively. The primary reason for the poor accuracy in the identification of debris flows was their location on the landscape, specifically, in deep gullies where shadow had a detrimental effect on the segmentation process. These results strongly support the viability of using high spatial resolution satellite remote sensing data and digital elevation models to create landslide inventories. However, the method is highly dependent upon the vegetative disruption associated with landslides. It may therefore be less applicable in arid regions or in regions with a low tree line.

## Acknowledgments

This research was funded by the Natural Sciences and Engineering Research Council of Canada. June Ryder is thanked for her assistance with aerial photographic interpretation.

## References

Baeza, C., and J. Corominas, 2001. Assessment of shallow landslide susceptibility by means of multivariate statistical techniques, *Earth Surface Processes and Landforms*, 26:1251–1263.

Barlow, J., Y. Martin, and S. Franklin, 2003. Detecting translational landslide scars using segmentation of Landsat ETM+ and DEM data in the northern Cascade Mountains, British Columbia, *Canadian Journal of Remote Sensing*, 29(4):510–517.

Brardinoni, F., and M. Church, 2004. Representing the landslide magnitude-frequency relation: Capilano River Basin, British Columbia, *Earth Surface Processes and Landforms*, 29: 115–124.

Brardinoni, F., O. Slaymaker, and M. Hassan, 2002. Landslide inventory in a rugged forested watershed: A comparison between air photo and field survey data, *Geomorphology*, 54:179–196.

Campbell, D., and M. Church, 2004. Reconnaissance sediment budgets for Lynn Valley, British Columbia: Holocene and

contemporary time scales, *Canadian Journal of Earth Sciences*, 40(5):701–713.

Chubey, M., S. Franklin, and M. Wulder, 2006. Object-based analysis of Ikonos-2 imagery for extraction of forest inventory parameters, *Photogrammetric Engineering & Remote Sensing*, 72(4): 383–394.

Congalton, R., 1991. A review of assessing the accuracy of classifications of remotely sensed data, *Remote Sensing and Environment*, 37:35–46.

Cruden, D., and D. Varnes, 1996. Landslide types and processes, *Landslides Investigation and Mitigation*, (K. Turner and R. Schuster, editors), Transportation Research Board Special Report 247, National Academy Press, Washington D.C., pp. 36–75.

Definiens, 2005. *eCognition User Manual*, Version 3, URL: http://www.definiens.com/documents/index.htm, (last date accessed: 15 March 2006).

Epp, H., and L. Beaven, 1988. Mapping slope failure tracks with digital Thematic Mapper data, *IGARSS'88: Proceedings of the International Geoscience and Remote Sensing Symposium*, 13–15 September, Edinburgh, Scotland, IEEE, New York, Vol. 3, pp. 1649–1652.

Environment Canada, 2005. URL: http://climate.weatheroffice.ec.gc.ca/climateData/canada_e.html, (last date accessed: 15 March 2006).

Evans, I., 1980. An integrated system of terrain analysis and slope mapping, *Zeitschrift fur Geomorphologie*, 36:274–295.

Gao, J., 1993. Identification of topographic settings conducive to landsliding from DEM in Nelson County, Virginia, *Earth Surface Processes and Landforms*, 18:579–591.

Geobase, 2005. Canadian Digital Elevation Data, URL: http://www.geobase.ca, (last date accessed: 15 March 2006).

Giles, P., M. Chapman, and S. Franklin, 1994. Incorporation of a digital elevation model derived from stereoscopic satellite imagery in automated terrain analysis, *Computers and Geoscience*, 20(4):441–460.

Giles, P., and S. Franklin, 1998. An automated approach to the classification of slope units using digital data, *Geomorphology*, 21:251–264.

Guthrie, R., and S. Evans, 2004. Analysis of landslide frequencies and characteristics in a natural system, Coastal British Columbia, *Earth Surface Processes and Landforms*, 29(11): 1321–1339.

Guzzetti, F., B. Malamud, D. Turcotte, and P. Reichenbach, 2002. Power-law correlations of landslide areas in central Italy, *Earth and Planetary Science Letters*, 195:169–183.

Haralick, R., K. Shanmugam, and D. Itshak, 1973. Textural features for image classification, *IEEE Transactions on Systems, Man, and Cybernetics*, 6:610–621.

Hovius, N., C. Stark, and P. Allen, 1997. Sediment flux from a mountain belt derived by landslide mapping, *Geology*, 25:231–234.

Iverson, R., 1997. The physics of debris flows, *Reviews of Geophysics*, 35(3):245–296.

Jones, K., 1998. A comparison of algorithms used to compute hill slope as a property of the DEM, *Computers and Geosciences*, 24(4):315–325.

Kidwell, K., 1990. *Global Vegetation Index User's Guide*, U.S. Department of Commerce/National Oceanic and Atmospheric Administration/National Environmental Data and Information Service/National Climactic Data Centre/Satellite Data Services Division.

Jacob, M., 2000. The impacts of logging on landslide activity at Clayoquot Sound, British Columbia, *Catena*, 38:279–300.

Martin, Y., K. Rood, J. Schwab, and M. Church, 2002. Sediment transfer by shallow landsliding in the Queen Charlotte Islands, British Columbia, *Canadian Journal of Earth Sciences*, 39(2): 189–205.

Martin, Y., and S. Franklin, 2005. Classification of soil- and bedrock-dominated landslides in British Columbia using segmentation of satellite imagery and DEM data, *International Journal of Remote Sensing*, 26(7):1505–1510.

Martin, Y., 2000. Modelling hillslope evolution: linear and nonlinear transport relations, *Geomorphology*, 34:1–21.

Massey, N.W.D., D.G. MacIntyre, and P.J. Desjardins, 2003. *Digital Geology Map of British Columbia: Tile NM10 Southwest B.C.*, B.C. Ministry of Energy and Mines, Geofile 2005-3, URL: http://www.em.gov.bc.ca/Mining/Geolsurv/Publications, (last date accessed: 15 March 2006).

McDermid, G., and S. Franklin, 1995. Remote sensing and geomorphic discrimination of slope processes, *Zeitschrift fur Geomorphologie*, 101:165–185.

Saunders I., J. Clague, and M. Robets, 1987. Deglaciation of Chilliwack River Valley, British Columbia, *Canadian Journal of Earth Sciences*, 24:915–923.

Sauchyn, D., and N. Trench, 1978. Landsat applied to landslide mapping, *Photogrammetric Engineering & Remote Sensing*, 44:735–741.

(Received 04 March 2005; accepted 10 May 2005; revised 16 June 2005)